POLITECNICO DI TORINO
Repository ISTITUZIONALE

Global/local models of composite laminated structures coupling classical 2D finite elements and arbitrarily large refined analysis subdomains

Terms of use:

Publisher copyright

(Article begins on next page)
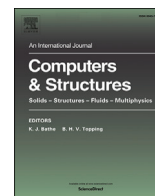
19 November 2024

Global/local models of composite laminated structures coupling classical 2D finite elements and arbitrarily large refined analysis subdomains

M. Enea [a], R. Augello [a], A. Pagani [a,*], E. Carrera [a,b]

[a] MUL² group, Department of Mechanical and Aerospace Engineering, Politecnico di Torino, Corso Duca degli Abruzzi 24, 10129 Torino, Italy
[b] Department of Mechanical Engineering, College of Engineering, Prince Mohammad Bin Fahd University, P.O. Box 1664, Al Khobar 31952, Kingdom of Saudi Arabia

ARTICLE INFO

ABSTRACT

The present paper introduces a global/local approach for the analysis of three-dimensional (3D) stress states of composite laminated structures. It consists of a two-step procedure. In particular, the first step makes use of finite element modeling based on classical 2D plate elements, whereas a refined layer-wise model based on Carrera Unified Formulation (CUF) is adopted to extract the 3D stress and strain fields in some critical regions that may have arbitrary dimensions. This approach allows dealing with large local areas, increasing the accuracy of the static solution, along with the possibility of embedding this technique in more complex procedures, such as the least-weight design of large heterogeneous complex assemblies, stiffness optimization, or localized progressive failure analysis. The numerical results shown in this paper want to assess the physical and numerical validity of the global/local approach. Particular attention is focused on the choice of the dimensions of the local area (patch) subjected to detailed refined analysis. Also, the convergence properties of the present hybrid FE model are discussed. The first examples deal with laminated composites. Then, the advantages of this methodology are further highlighted by considering free-edge problems and a complex wing structure.

1. Introduction

Composite structures are nowadays widely used in aeronautical applications due to their specific mechanical performances. However, due to the huge computational cost required, a significant shortcoming in the design and analysis of composite structures is the difficulty of developing an accurate numerical model. In fact, a typical composite laminate can reach a scale ratio between the main dimension and the single-ply thickness of 10^4. Generally, the finite element method (FEM) is used to predict the structural behavior of composite laminates. However, the large-scale ratio value leads to highly time-consuming mathematical models, especially if three-dimensional (3D) elements are adopted. In fact, some research (e.g., [1]) demonstrated the necessity of at least three elements for each layer through the laminate thickness for an accurate solution. Thus, two-dimensional (2D) elements are widely used to analyze thin composite laminates to reduce the computational demand. Nevertheless, results provided by 2D investigations are unreliable when stress concentrations or free-edge effects occur, since they require a 3D description of the problem.

In this context, researchers proposed different solutions to tackle this problem, among which the global/local approach stands out. This technique can provide a reduction in terms of simulation time, keeping a high level of accuracy. Early research works developed in the past decades with limited computing power were successfully applied to linear [2–5] and non-linear [6,7] analysis. Two categories of global/local methods are proposed in the literature, namely, two-way and one-way coupling approaches. The first approach involves exchanging information between global and local models in both directions. Some examples of two-way couplings are represented by the so-called h-refinement [8] and p-refinement [9] methods, which result in the use of different mesh sizes and polynomial degrees, respectively. A combination of these two approaches is the so-called hp-refinement method, presented by Babuska and Dorr in [10]. Hühne et al. propose a two-way global–local technique based on the shell-to-solid submodeling feature to investigate buckling and intralaminar damage behavior in composite panels [11]. This approach is extended by Akterskaia et al. to investigate the progressive failure and debonding [12,13]. These works adopt a loosely-coupled approach, meaning that global and local analyses

---

* Corresponding author.

E-mail addresses: marco.enea@polito.it (M. Enea), riccardo.augello@polito.it (R. Augello), alfonso.pagani@polito.it (A. Pagani), erasmo.carrera@polito.it (E. Carrera).
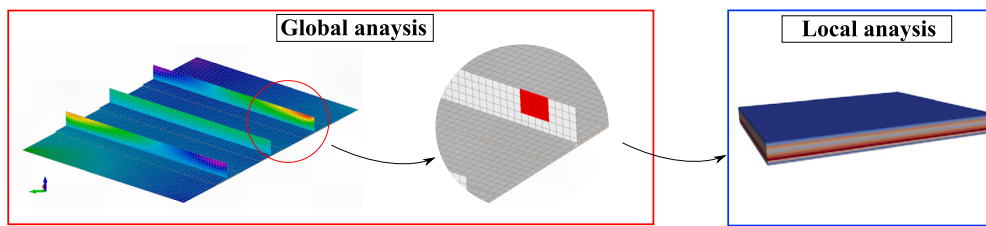
Fig. 1. Application of the two-step global/local approach on an aeronautical reinforced panel. The first step consists in the static analysis of the whole structure by means of classical 2D finite elements, whereas the local one involves a refined LW model of a region of interest for the panel.

are performed sequentially. A different class of two-way global/local techniques is based on strong/tight coupling between global and local models. According to this approach, global and local domains of the structure are discretized with different levels of refinements. They are connected at the global/local interface using various techniques, such as, for instance, tie-constraints. Thus, a single numerical model is obtained, leading to the solution of the global and local models simultaneously. Krueger et al. employ such a technique to study delamination in composite laminates [14] and stiffener-skin debonding [15]. Multipoint constraints are used at the interface between the global and local regions. Similar strongly-coupled global–local approaches have been used recently to investigate progressive damage in composite laminates subjected to low-velocity impact [16,17]. Other examples of two-way coupling global/local techniques are represented by the multi-grid method [18] and the Arlequin method [19].

A second class of global–local methods is represented by one-way approaches. In these techniques, information is transferred only from the global model to the refined local model once. An example is proposed in [20], where the authors combine a progressive failure technique with a submodeling method. Gendre et al. in [21] introduce a global/local strategy consisting of a global linear model of the entire structure and a local non-linear model. Vescovini et al. in [22] propose a global/local technique for failure analysis of composite multi-stringer panels. A coarse global mesh is employed for the panel, along with a local model adopting cohesive elements to capture the delamination failure modes. Finally, Orifici et al. [23] introduce a computationally efficient two-step global/local approach to identify interlaminar damage initiation.

The global/local approaches can be applied for a more reliable stress analysis of a composite laminate. More specifically, phenomena that may occur within a composite structure, i.e., free-edge effects and failure, demand a 3D description of the stress distribution. Thus, 3D solid elements can be used at the local level [24]. If a typical aeronautical lay-up with tens of layers is considered, even a relatively small region analysis leads to a considerable number of solid elements. Therefore, aircraft companies and composite designers must rely on experimental rules, such as the Angle Minus Longitudinal (AML) method [25]. Furthermore, classical theories cannot accurately describe the 3D effects that arise at the free-edge of a composite laminate due to the mismatch of the mechanical properties of different ply in a composite laminate.

For these reasons, in this work, a global/local approach with one-way coupling is presented, where the global analysis is performed using commercial software, and then a local region is investigated using advanced layer-wise (LW) models with Carrera Unified Formulation (CUF) formalism [26]. CUF models have been shown to assure excellent efficacy and computational efficiency in evaluating complex 3D stress states in composite structures [27,28]. This strategy provides accurate solutions for stress and strain transverse components, which can be essential when the onset of failure in laminates has to be predicted. Recent works [29,30] have shown this global/local approach's capability to accurately recover the 3D stress state at the ply level. However, in these researches, a so-called element-wise (EW) formulation is used, meaning that a single global element can be chosen as the local area to be analyzed through advanced LW theories, leading to some limitations in

terms of accuracy and dimension of the region to locally refine. Therefore, the present work aims to extend this global/local approach to a patch-wise (PW) formulation. In this case, the local region to be refined can be chosen as large as required. A patch of elements can be selected, and information from all the global nodes at the local area interface is employed as boundary conditions for the LW model. This extension allows the analysis of more significant regions in a complex structure and the evaluation of 3D stress states and failure onset while reducing the computational demand of the analysis. The PW formulation can help in exploiting the potential of this global/local approach to be embedded in more complex analysis, such as optimization loops for failure index or stress concentration factor minimization (as in [31]) in critical domains of a large structure. Recently, two different strategies for coupling between higher-order CUF-based elements and 3D peridynamics (PD) have been proposed [32,33], where PD is a non-local theory based on integro-differential equations. Pagani et al. [34] recently adopted one of these coupling technique for progressive failure analysis. Further development of the present work could be represented by combining the global/local PW approach with a PD-based model for localized progressive failure analysis.

The organization of this paper is the following: first, the global/local approach is introduced in Section 2, along with a focus on numerical models adopted for global and local analysis. Then, numerical results are shown and discussed in Section 3. Finally, the main conclusions are drawn.

2. Global/local approach

2.1. Two-step procedure

The global/local strategy adopted in this work consists of two steps (see Fig. 1), which can be summarized in the following way:

1. **A global analysis on a composite laminate is conducted**. The commercial software Nastran [35] is used to perform the analysis of the full structure. This step is recalled as global analysis. Classical CQUAD4 elements are adopted in combination with PCOMP properties for the geometrical and material descriptions, respectively. The acronym PCOMP refers to the properties of a n-ply composite material laminate, whereas CQUAD4 are four-node two-dimensional elements that make use of First Shear order Deformation theory (FSDT) [36], according to which the displacement field is given as follows:

$$
\begin{aligned}
u_1(x, y, z) &= u(x, y) + z\varphi_x \\
u_2(x, y, z) &= v(x, y) + z\varphi_y \\
u_3(x, y, z) &= w(x, y)
\end{aligned}
\tag{1}
$$

where u, v, w, φ_x and φ_y are five unknown displacement functions of the midplane of the plate. The key contribution of this study is the expansion of the CUF-based global/local analysis approach to include a patch-wise (PW) formulation. This novel approach enables the selection of a group of global elements for local analysis, providing more accurate results than the traditional element-wise (EW) approach, where only a single CQUAD element is locally re-
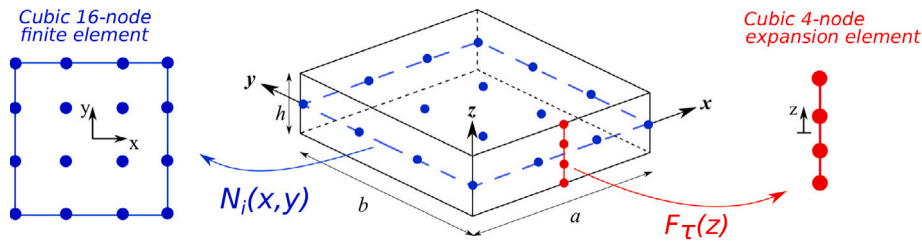
Fig. 2. Graphical representation of the cubic interpolation for in-plane and thickness domains.

fined at a time. Notably, prior research [30,37] has only explored the EW approach within the CUF framework.

2. **A local analysis on the domain elements is performed**. The refined local analysis is conducted using high-order 2D plate finite elements based on the Carrera Unified Formulation (CUF), that allows a straightforward development of higher-order models in a hierarchical and automatic manner within a finite element domain. The 3D displacement field $\mathbf{u}(x, y, z)$ is thus defined as a 1D through-the-thickness expansion function of the primary unknowns, evaluated via the finite element method. The relation can be written as follows:

$$\mathbf{u}(x, y, z) = F_\tau(z) N_i(x, y) \mathbf{q}_{\tau i} \tag{2}$$

where F_τ is the expansion function, N_i the shape function and $\mathbf{q}_{\tau i}$ the nodal unknowns vector. Index τ represents the number of terms in the thickness expansion, whereas the subscript i denotes the number of structural finite element nodes. This research adopts 2D sixteen-nodes cubic elements (Q16) as shape functions for the in-plane modeling. Cubic Lagrange polynomials are employed as F_τ function (LE). This work adopts the four-node cubic Lagrange expansion function (LD3) over the thickness, where LD stands for Lagrange Displacement-based (see Fig. 2). More information about Lagrange polynomials can be found in [38].

The derivation of the governing equations for the elasticity problem is made by means of the Principle of Virtual Displacements (PVD). For a static problem, it reads:

$$\delta L_{int} = \delta L_{ext} \tag{3}$$

where δL_{int} and δL_{ext} represent the virtual variation of the strain energy and the virtual variation of the work of external loads. The term related to the internal strain energy can be written as follows:

$$\delta L_{int} = \int_V \delta \boldsymbol{\epsilon}^{\mathrm{T}} \boldsymbol{\sigma} \, dV \tag{4}$$

where $\boldsymbol{\epsilon}$ and $\boldsymbol{\sigma}$ are the strain and stress vector, respectively, and V is the volume of the body. By introducing the strain-displacement relations, the virtual variation of the strain energy can be written in a compact form:

$$\delta L_{int} = \delta \mathbf{q}_{sj}^T \mathbf{k}^{ij\tau s} \mathbf{q}_{\tau i} \tag{5}$$

where $\mathbf{k}^{ij\tau s}$ is a 3×3 matrix called Fundamental Nucleus (FN) of the structural stiffness matrix. For the sake of clarity, the $k_{ij\tau s}^{xx}$ component is reported below:

$$k_{xx}^{ij\tau s} = \int_V \tilde{C}_{11} \frac{\partial}{\partial x}(N_j F_s) \frac{\partial}{\partial x}(N_i F_\tau) dV + \int_V \tilde{C}_{16} \frac{\partial}{\partial x}(N_j F_s) \frac{\partial}{\partial y}(N_i F_\tau) dV$$

$$+ \int_V \tilde{C}_{44} \frac{\partial}{\partial z}(N_j F_s) \frac{\partial}{\partial z}(N_i F_\tau) dV + \int_V \tilde{C}_{16} \frac{\partial}{\partial y}(N_j F_s) \frac{\partial}{\partial x}(N_i F_\tau) dV$$

$$+ \int_V \tilde{C}_{66} \frac{\partial}{\partial y}(N_j F_s) \frac{\partial}{\partial y}(N_i F_\tau) dV$$

$$\tag{6}$$

The remaining components of the FN can be retrieved in the same manner (see [26]). It should be noted that the formal expression of the FN remains invariable with respect to the structural theory or FE scheme chosen. Therefore, by simply looping on the indexes τ, i, j, s, any structural model can be created.

It should be highlighted that the validity of results over the local region is guaranteed far from the borders of the region. Some attention has to be paid at the boundaries, due to the fact that a coupling between different structural kinematics (FSDT for global scale, high-order for local scale) is performed. Thus, some distortions at boundaries can arise, without any macroscopic effect on strain and stress evaluation.

2.2. Local displacement-based model

The CUF model used for the analysis of the local domain is a displacement-based formulation, meaning that pure displacement Degrees of Freedom (DOFs) at each node are considered. Nevertheless, the commercial software provides translational displacements (u_x^0, u_y^0, u_z^0) and rotations $(\theta_x^0, \theta_y^0, \theta_z^0)$ at each node of the global model. Thus, a suitable procedure must be implemented to transform the global model's rotations into pure displacement DOFs. The chosen strategy is the same adopted in previous works [30,37], where a Reissner-Mindlin displacement field [39,40] is employed for the computation of translational displacements at the local model boundaries. The Reissner-Mindlin displacement field which operates is written as follows:

$$\boxed{u_x}(x, y, z) = \boxed{u_x^0}(x, y) + z\boxed{\theta_y^0}(x, y) - y\boxed{\theta_z^0}(x, y)$$

$$\boxed{u_y}(x, y, z) = \boxed{u_y^0}(x, y) - z\boxed{\theta_x^0}(x, y) + x\boxed{\theta_y^0}(x, y) \tag{7}$$

$$\boxed{u_z}(x, y, z) = \boxed{u_z^0}(x, y) - x\boxed{\theta_y^0}(x, y) + y\boxed{\theta_x^0}(x, y)$$

where the circled quantities u_x^0, u_y^0, u_z^0 and $\theta_x^0, \theta_y^0, \theta_z^0$ are displacements and rotations of the global model, whereas the boxed ones u_x, u_y, u_z are the pure translational displacement DOFs in the refined model. The graphical representation of these transformations is shown in Fig. 3.

2.3. Patch-wise formulation

A common procedure for EW and PW formulations consists of the computation of displacements in all interface nodes using quantities from the global model. These displacements are then employed as boundary conditions for the local model. Nevertheless, in the precedent EW formulation, displacements and rotations from a single chosen CQUAD element were adopted as boundary conditions. On the other hand, in the present PW formulation, displacements and rotations from all the involved global nodes are considered and used to construct the boundary condition set. An example of the procedure is illustrated in Fig. 4., which also reports the EW approach. On the right, a local region identified by a 2×2 patch of elements is considered. The two areas have the same geometrical dimensions. Let us consider a point at the quarter $(L/4, 0)$ of the edge described by global nodes 1 and 2. Concerning the EW approach, displacements and rotations evaluated in the point x_{EW} result from the interpolation within the single element CQUAD, referred to as 1_{EW}, which describes the entire region. On the other hand, for
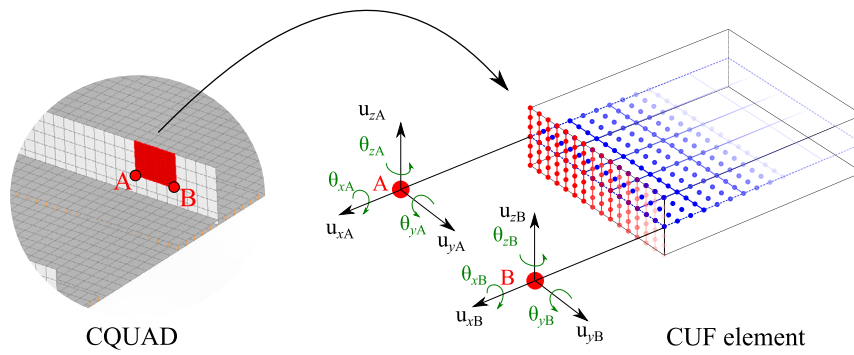
Fig. 3. Graphical representation of the procedure to transform rotational DOFs of the global model into pure displacement for local one. The evaluated displacements, i.e. the boxed u_x, u_y, u_z of Eq. (7) are used as boundary condition of the local element. Two LD3 are used for thickness modeling in the local domain in this figure.
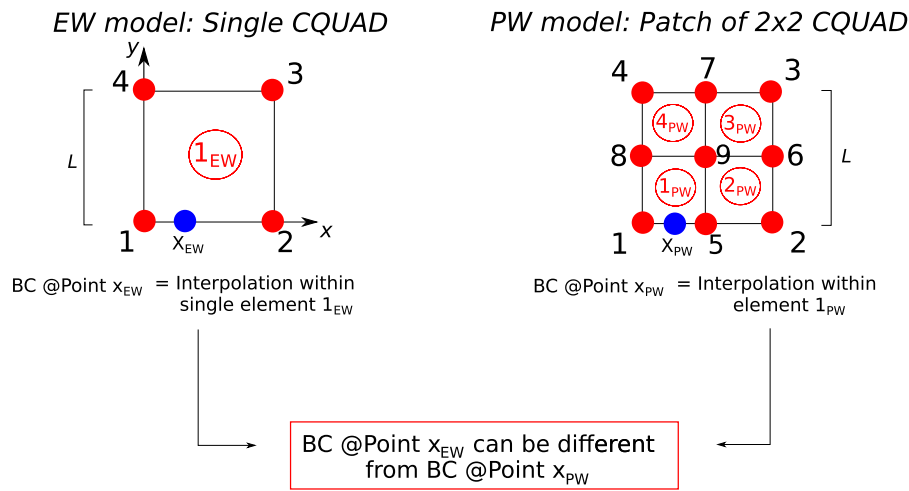

Fig. 4. Differences between element-wise and patch-wise formulation in terms of boundary conditions evaluation.
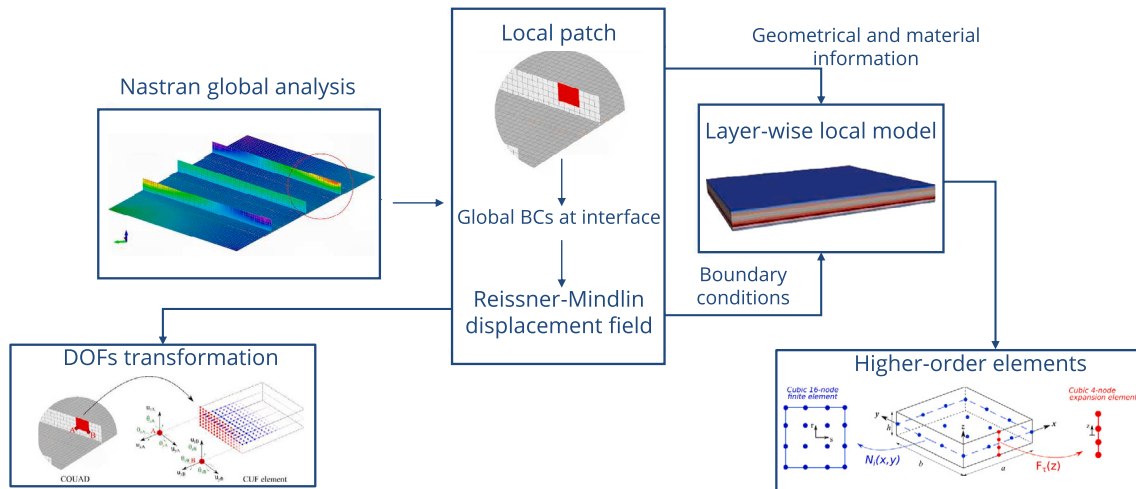

Fig. 5. General procedure for the present two-step global approach. The first step is represented bt the global analysis of a complex structure using 2D plate finite elements. The middle rectangle shows the operations acting as interface between the global and local models. The rectangle on the right represents the refined local model to be analyzed. The output of this procedure is the strain and stress states in the chosen patch of elements.

the PW model, boundary conditions in point x_{PW} are obtained through interpolation within element 1_{PW}. Refining the global mesh without altering the geometrical dimensions of the local region will facilitate the provision of more precise boundary conditions, resulting in a more accurate assessment of stress components.

A graphical representation of the entire procedure is shown in Fig. 5.

3. Numerical results

Numerical results obtained with the global/local approach introduced in this work are shown. Its capability is demonstrated by analyzing two-layer and ten-layer composite plates. For each example, the influence of the global and local meshes is investigated by performing convergence analyses, and the results are compared to those coming
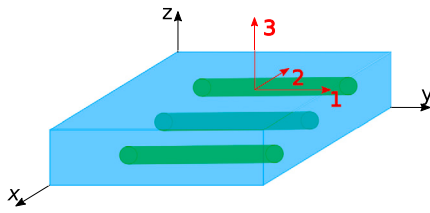
Fig. 6. Global (in black) and material (in red) reference frames. Direction 1 for the material frame represents the fiber direction, whereas 2 and 3 are the transversal directions.
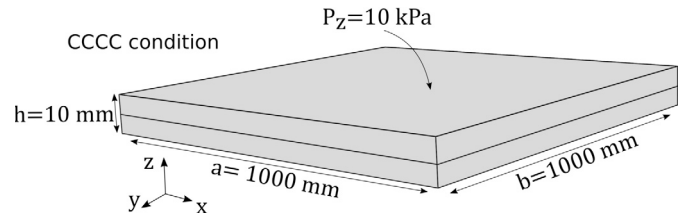

Fig. 7. Geometrical and modeling features of the investigated plate.
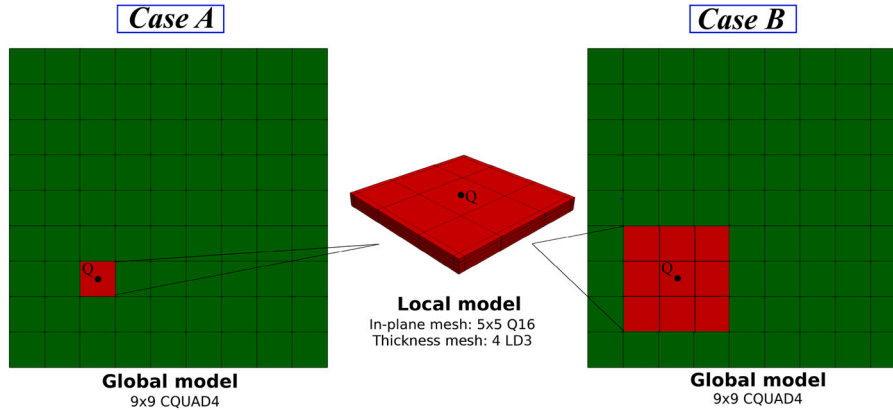

Fig. 8. Global and local models of the two-layer plate subjected to transverse pressure. Case A represents the EW approach, whereas a PW approach for a 3 x 3 elements region is recalled as Case B. Point Q represents the evaluation point of stress components.

Table 1
Material properties in MPa.

E_{11}	E_{22}	E_{33}	v_{12}	v_{13}	v_{23}	G_{12}	G_{13}	G_{23}
143.17	9.64	9.64	0.252	0.252	0.49	6.09	6.09	3.12

Table 2
Material allowables in MPa.

X_T	X_C	Y_T	Y_C	XY	XZ	YZ
2586.0	1620.0	94.0	340.5	174.5	152.6	174.5

from refined layer-wise models. Furthermore, an analysis of a free-edge case is conducted, with the out-of-plane components of the stress tensor being evaluated using different patch dimensions and discretization. Finally, an aeronautical wing under bending load is considered. These analyses provide insight into the performance of the PW approach under varying conditions and further demonstrate its potential for accurate and efficient global/local analysis of complex structures. The stresses retrieved from the local refined analysis are reported in the global or material reference system. A graphical representation is shown in Fig. 6.

3.1. Two-layer plate subjected to transversal pressure

The first case study is a two-layer plate subjected to transversal pressure, with [90°/0°] stacking sequence. The plies are of equal thickness and are made of an orthotropic material, whose properties are enlisted in Table 1, whereas allowable values are detailed in Table 2. Geometrical features and boundary conditions are shown in Fig. 7. A transversal pressure is applied on the surface of the laminate, with a magnitude equal to 10 kPa. All four edges are in clamped conditions.

This numerical case serves as an assessment of the proposed PW formulation. The model for the first step of the global/local analysis consists of 81 CQUAD4 elements. Then, two different regions are chosen for the local study, a single global element for case A (see Fig. 8(a)) and

a 3×3 patch in case B (see Fig. 8(b)). Both regions are locally refined with high-order finite elements, adopting a 5×5 grid of cubic Q16 in the plane and two LD3 for each layer through the thickness. The in-plane discretization of the local domain is represented by a grid built using Chebyshev nodes distribution to minimize errors that occur at edges when using polynomial interpolation [41]. A comparison with the EW global/local approach and a full layer-wise model is provided. The latter is built with a total of 196 cubic Q16 elements for the in-plane mesh, while four-node cubic LD3 are adopted through the thickness of the plate, two for each layer. Strain and stress distributions are evaluated in point Q ($\frac{a}{4}$, $\frac{b}{4}$), which corresponds to the centroid for both the single element and the 3×3 patch.

Fig. 9 shows the in-plane stress through the laminate thickness in point Q for the layer-wise model and the two cases of global/local analysis. Results obtained in cases A and B perfectly match those obtained through a refined model. Thus, in this specific case, it can be concluded that displacements and rotations extracted from the global model are sufficient as boundary conditions for the refined local analysis to retrieve the correct in-plane stress state of the laminate. Nevertheless, this consideration is not valid when out-of-plane stresses are evaluated (see Fig. 10). In fact, a slight discrepancy is witnessed for both σ_{xz} and σ_{yz} between case A and the LW model. This error is mitigated when a larger global region is chosen to be locally analyzed, as in case B. As a result, a larger global area can help provide a more accurate set of boundary conditions for the local model, thanks to the more significant number of global nodes involved. It is important to note that for each global/local approach considered (Case A or B), the transverse shear stresses fulfill the C_z^0 requirements [42] and are null at the thickness edges. It should be underlined that the σ_{zz} component is not herein represented due to its very small value compared to other stress components.

A failure analysis is also performed. Failure Indices (FIs) are evaluated at point Q for each case using the Hashin 3D criterion [43]. The stress components obtained from the local analysis are used as input to evaluate the four Hashin based FIs, namely fiber tension, fiber compression, matrix tension and matrix compression. The results are shown in Fig. 11. The values obtained in cases A and B are consistent with the full
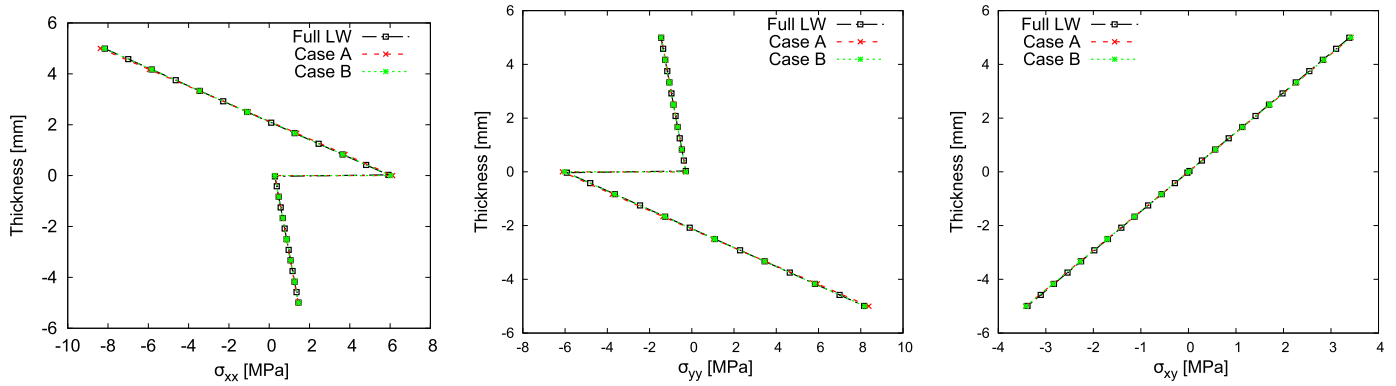
Fig. 9. Comparison of in-plane stresses distribution through the thickness of the laminate with $a/h = 100$ between a full LW model and two global/local approaches (see Case A and B in Fig. 8).
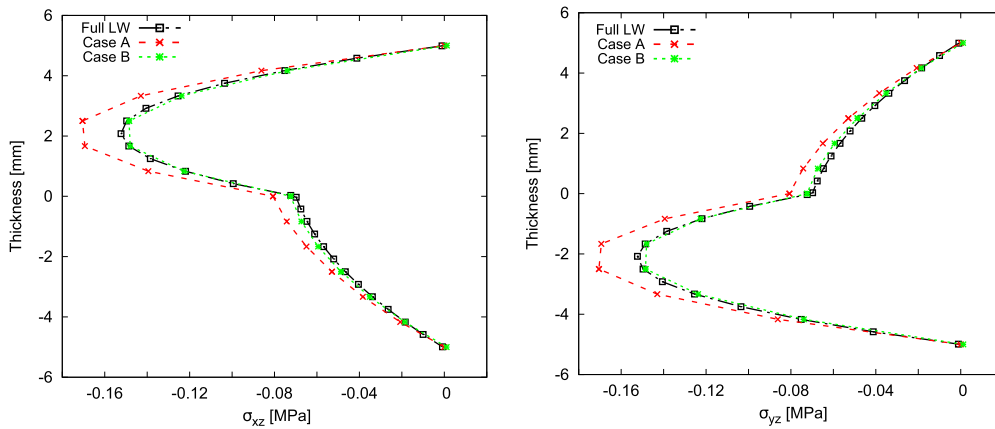

Fig. 10. Comparison of transverse shear stresses evolution through the thickness of the laminate with $a/h = 100$ between a full LW model and two global/local approaches (see Case A and B in Fig. 8).

LW model. It is noteworthy that no significant differences are observed between the two global/local analyses, despite the slight discrepancy in the out-of-plane stress distribution (see Fig. 10). This is because the values of σ_{xz} and σ_{yz} are at least 100 times smaller than the in-plane stresses, resulting in a negligible influence of the out-of-plane stress values on the failure mechanism.

Finally, a plate with different slenderness ratio is considered, in order to prove the validity of the present approach when thick plates are considered. The in-plane dimensions are those expressed in Fig. 7, whereas a thickness of 100 mm is here considered, thus resulting in a slenderness ratio $a/h = 10$. For the sake of brevity, Fig. 12 depicts the transverse shear stresses for the investigated thick plate. A comparison between a full LW and a G/L patch-wise solution is proposed.

The outcomes clearly show how the efficacy of the proposed approach still applies when dealing with thick plates, being able to accurately describe the through-the-thickness behavior of transverse shear stresses.

3.2. Ten-layer composite plate subjected to a localized transverse pressure

The second case study consists of a ten-layer composite plate. The material and geometric properties are the same as those used in the previous case. A symmetric stacking sequence $[90/45/45/0/90]_s$ is chosen. A transversal pressure is applied only on a central squared region, with a side dimension equal to 110 mm. The plate is simply supported.

3.2.1. Global mesh convergence
A preliminary convergence study is carried out on the mesh size of the global model. An illustrative overview of the three investigated

cases is shown in Fig. 13. Briefly, we increase the refinement of the global model while maintaining the domain to be locally analyzed. Consequently, the local patch corresponds to a single global element for case A.1, a 2×2 patch for case B.1, and a 3×3 patch for case C.1. The local model adopted is the same for all three cases, consisting of a 5×5 grid of Q16 elements for in-plane mesh and a total of ten LD3 through the thickness, one for each layer. Stresses are evaluated at point $Q\left(\frac{a}{4}, \frac{b}{4}\right)$, and they are reported in the global reference system.

In-plane stress distributions are shown in Fig. 14. The convergence is reached with case B.1. It can be noticed that case A.1 already provides great overall accuracy. However, slight discrepancies can still be detected, such as σ_{xx} values in top and bottom layers or σ_{yy} behavior in 0°- oriented layers. Through-the-thickness stress distributions are displayed in Fig. 15. Full layerwise solution for σ_{xz} is matched when cases B.1 and C.1 are considered. On the other hand, the σ_{yz} is well reproduced by all models.

3.2.2. Local mesh convergence
A second convergence study is performed on the mesh refinement of the local model. A 9×9 grid of four-node plate elements is adopted for the global model, and a 3×3 patch of global elements is chosen for the local analysis, whose centroid is located in point Q. Three different in-plane meshes are employed for the refined local models. Information about the considered cases is summarized in Fig. 16.

Numerical results are shown in Fig. 17 for in-plane stresses and in Fig. 18 for the through-the-thickness components. A first important remark can be issued about the behavior of σ_{xx}. In fact, case A.2, representing the coarser local mesh, leads to significant differences in evaluating the normal stress at the top and bottom layers. On the other hand,
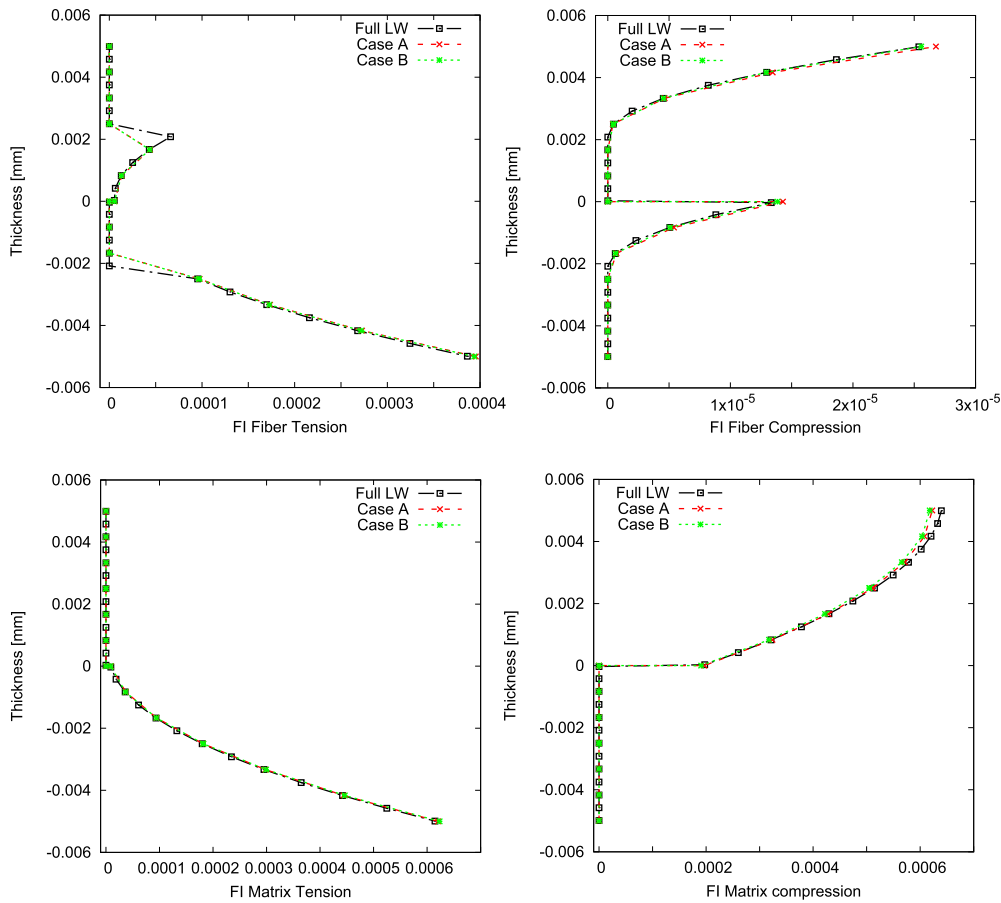
Fig. 11. Comparison of failure indices between a full LW model and two global/local approaches (see Case A and B in Fig. 8). Hashin 3D criterion has been applied for failure indices evaluation.
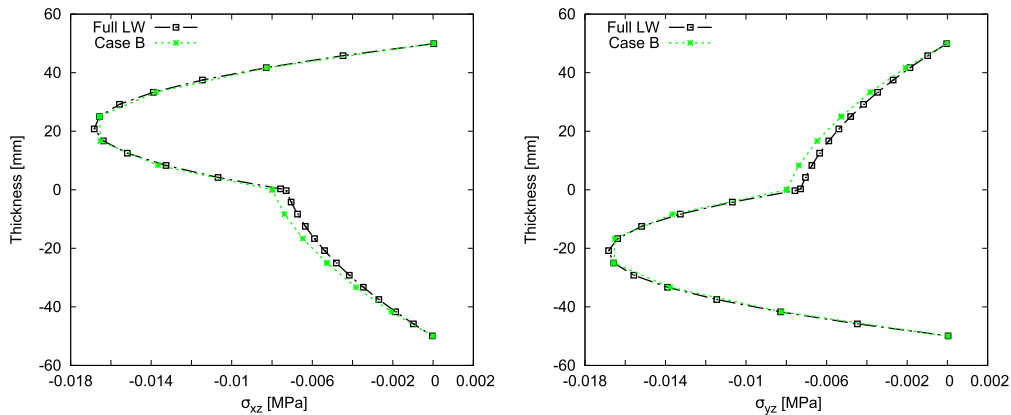

Fig. 12. Comparison of transverse shear stresses evolution through the thickness of the laminate with $a/h = 10$ between a full LW model and a global/local approach (see Case B in Fig. 8).

cases B.2 and C.2 match the results obtained via the full LW model. As in the previous case study, transverse shear stress components are 100 times lower than in-plane ones. The global/local approach still correctly reproduces the behavior of transverse stress components retrieved with the LW model.

3.2.3. Centroid convergence

A final convergence study is performed considering the patch size as a parameter. In this case, mesh refinement for global and local models is fixed. A model with 324 CQUAD4 plate elements is adopted, while

the local model is discretized with a 5×5 Q16 grid for the in-plane and ten LD3 through-the-thickness of the laminate. Thus, the only variable is the dimension of the patch to be locally analyzed. A single global element is considered in case A.3, whereas 3×3 and 5×5 patches of global elements are chosen for the local analysis in case B.3 and C.3, respectively. These regions have been chosen to have their centroids at the same coordinates. Fig. 19 shows the three global/local models with red regions highlighting the different patches.

Figs. 20 and 21 show the stress distributions for in-plane and out-of-plane components, respectively. It is evident that the single
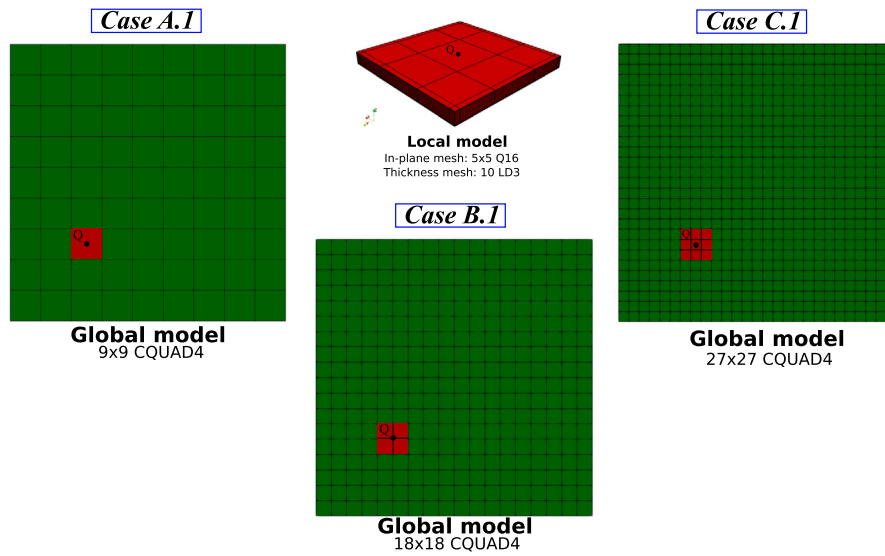
Fig. 13. Global and local models employed for global mesh convergence study. Patch of elements to be locally refined are highlighted in red. Point Q represents the evaluation point of stress components.
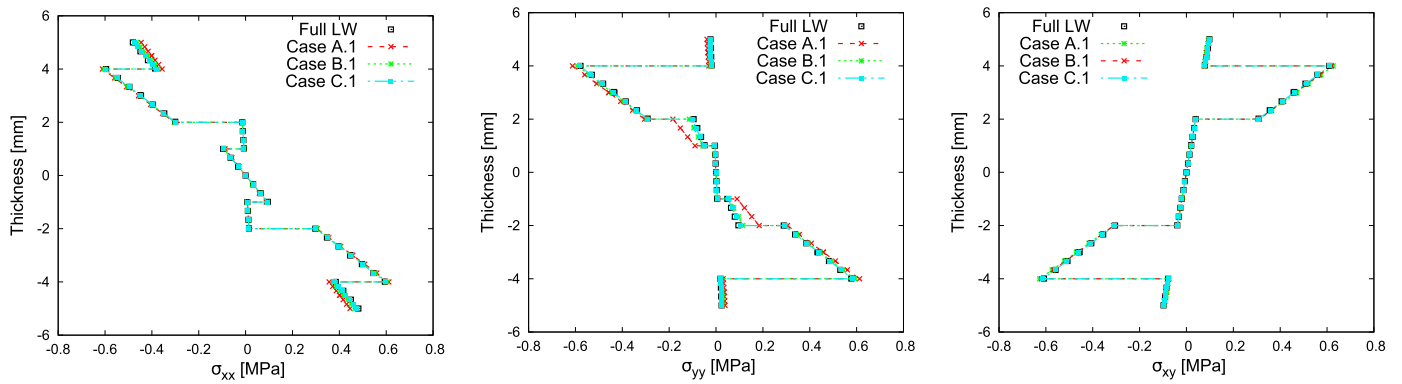

Fig. 14. Comparison of in-plane stresses evolution through the thickness of the laminate between a full LW model and three global/local models (see Case A.1, B.1 and C.1 in Fig. 13).

Fig. 15. Comparison of transverse shear stresses evolution through the thickness of the laminate between a full LW model and three global/local models (see Case A.1, B.1 and C.1 in Fig. 13).
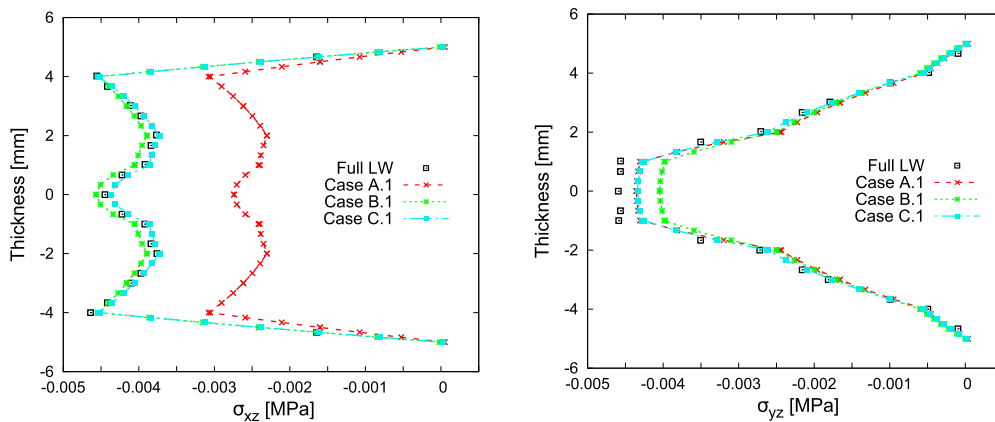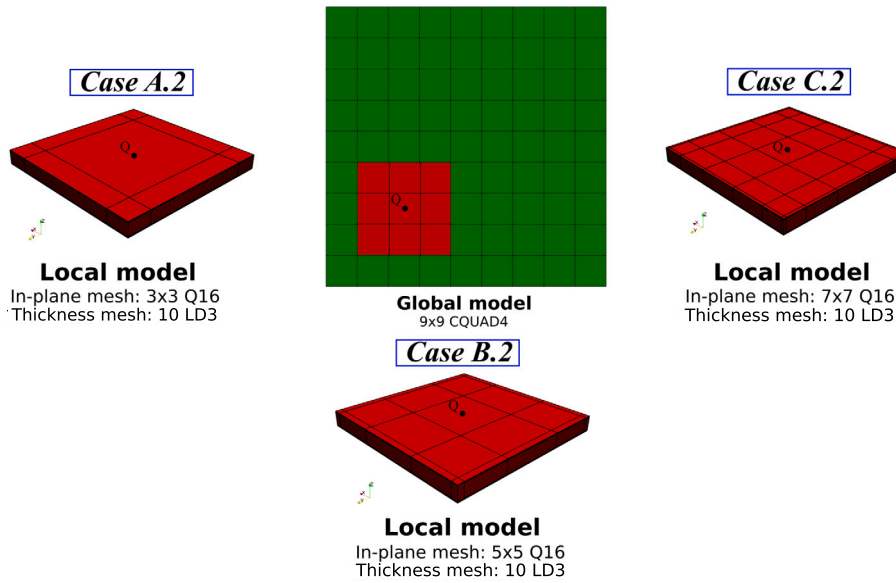
Fig. 16. Global and local models employed for local mesh convergence study. The patch of elements to be locally refined is highlighted in red. Point Q represents the evaluation point of stress components.
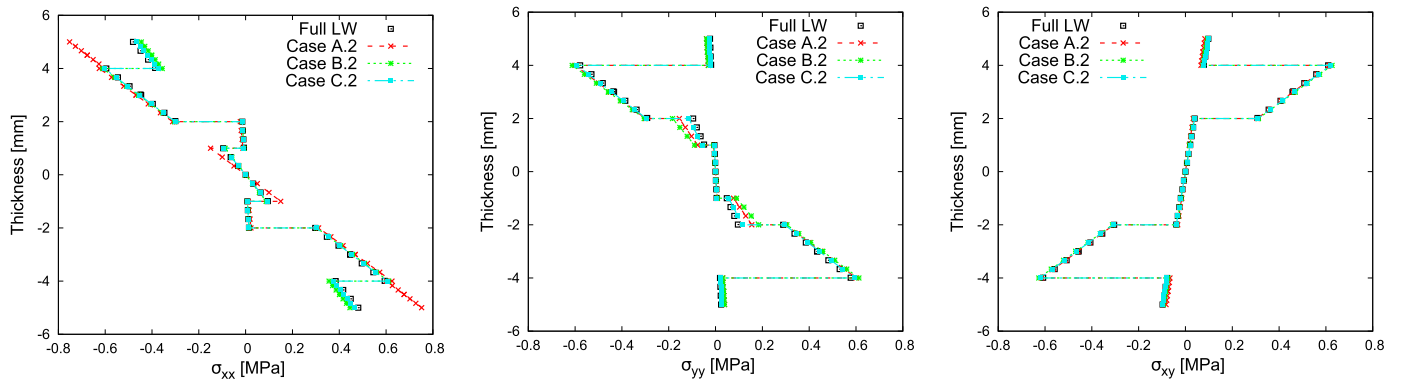

Fig. 17. Comparison of in-plane stresses distribution through the thickness of the laminate between a full LW model and three global/local models (see Case A.2, B.2 and C.2 in Fig. 16).
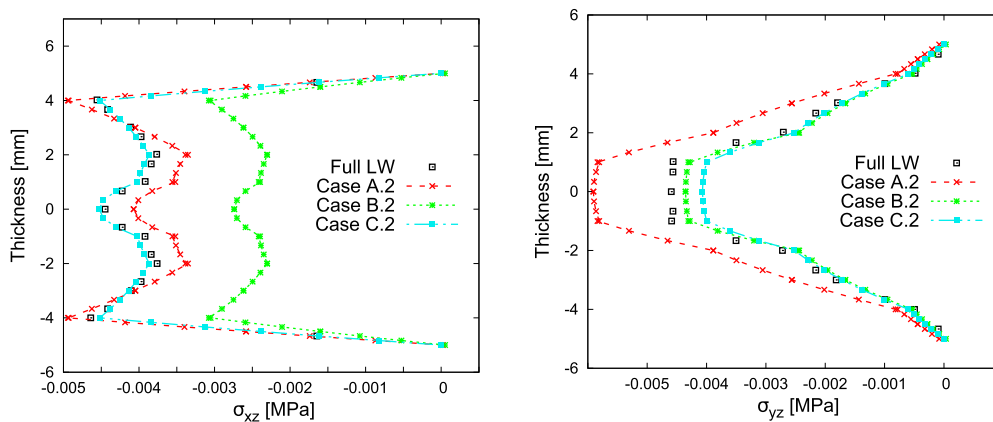

Fig. 18. Comparison of transverse shear stresses evolution through the thickness of the laminate between a full LW model and three global/local models (see Case A.2, B.2 and C.2 in Fig. 16).
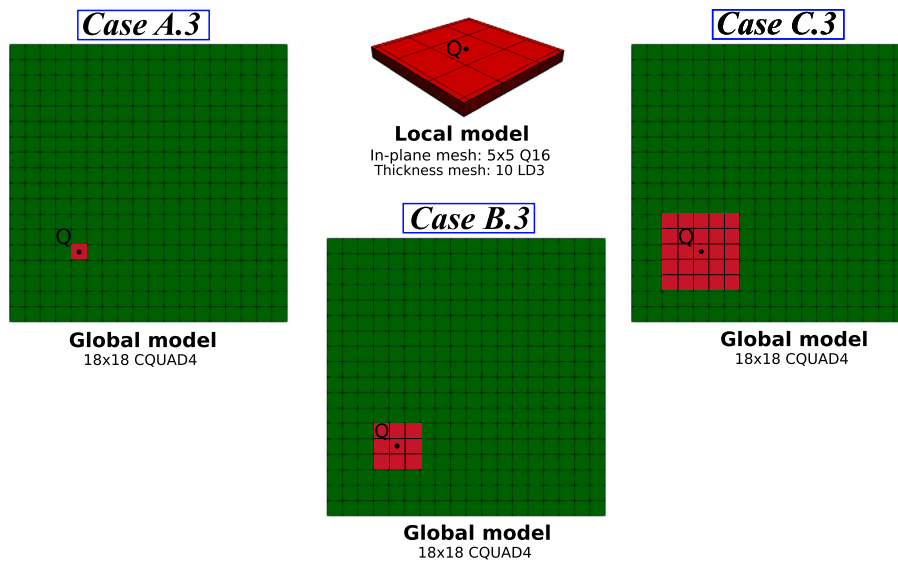
Fig. 19. Global and local model employed for patch size convergence study. Group of elements to be locally refined are highlighted in red.

Fig. 20. Comparison of in-plane stresses evolution through the thickness of the laminate between a full LW model and three global/local models (see Case A.3, B.3 and C.3 in Fig. 19).

Fig. 21. Comparison of transverse shear stresses evolution through the thickness of the laminate between a full LW model and three global/local models (see Case A.3, B.3 and C.3 in Fig. 19).
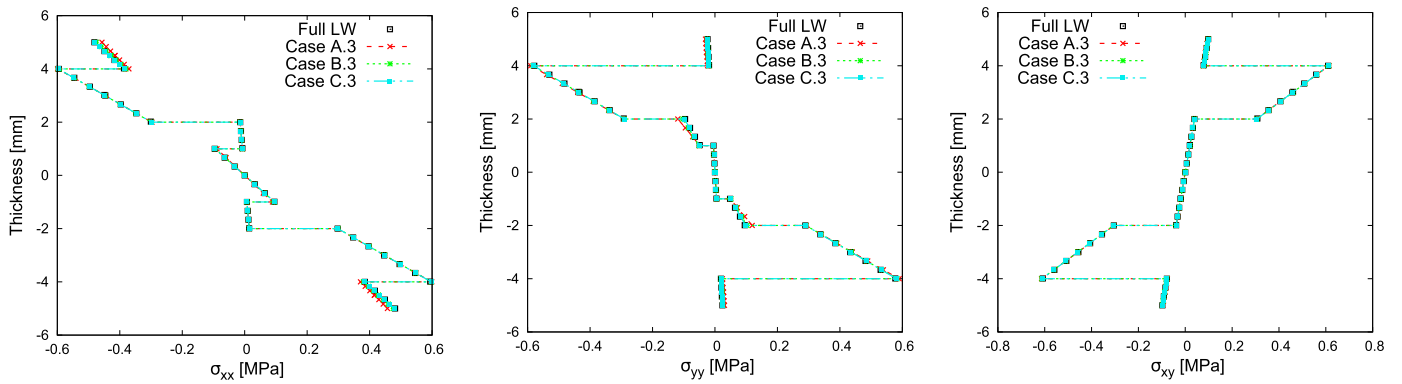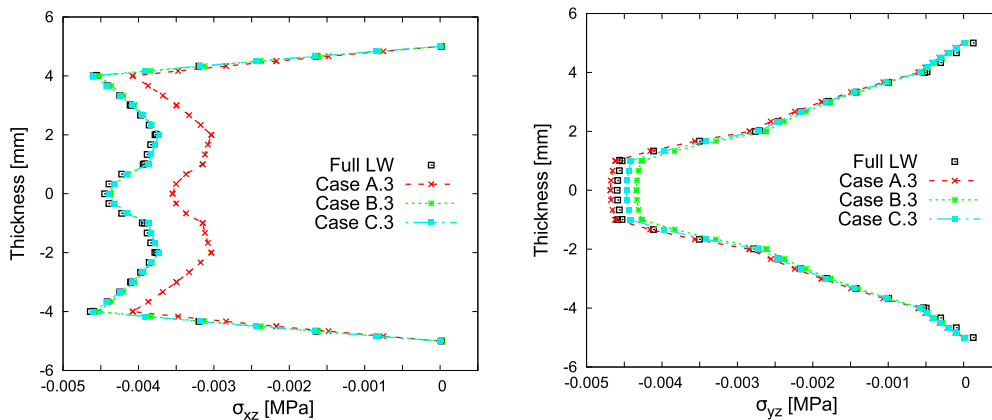
Table 3
Material properties in GPa.

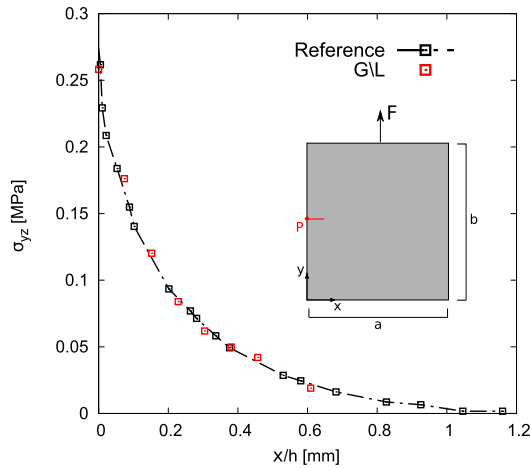| E_{11}	E_{22}	E_{33}	v_{12}	v_{13}	v_{23}	G_{12}	G_{13}	G_{23}
159.0	8.4	8.4	0.33	0.33	0.33	4.1	4.1	4.1

Fig. 22. Transverse shear stress along x at the plies interface 90/-15 for $y = b/2$. The horizontal axis starts at the free-edge (Point P) for $x/h = 0$ and goes towards the middle of the plate (along the red line). Reference solution is from [44].

global element can provide sufficient information to obtain an accurate stress distribution for in-plane components and shear stress σ_{yz}. On the other hand, in case B.3, the global/local model is needed to correctly reproduce the σ_{xz} evolution through the thickness of the laminate.

3.3. Free-edge analysis

The following case study shows the capability of this global/local approach to reproduce the free-edge effects that arise due to the mismatch of the mechanical properties of the plies at the interfaces. A composite plate from Lorriot et al. [44] is used as a reference. The shape of the plate is a rectangle with sides equal to $a = 200$ mm and $b = 300$ mm (see Fig. 22). The mechanical properties of the orthotropic material are enlisted in Table 3. The stacking sequence of the plate is $[15_2/90/-15_2]_s$, and each ply has a thickness of 0.125 mm. The loading conditions adopted in the reference work are simulated by imposing a clamped condition at coordinate $y = 0$ and applying a traction force of 250 N on the opposite edge. The global mesh discretization consists of 10 CQUAD along the x-direction and 15 elements along the y-direction. A single global element is chosen for this case, meaning that an EW strategy is adopted. The local mesh consists of a 5×5 Q16 elements for in-plane discretization, and a total of ten cubic LD3 through-the-thickness of the laminate, one for each layer of the plate.

Fig. 22 displays the distribution of the transverse shear stress σ_{yz}, starting from the free-edge (at $x/h = 0$) towards the inner part of the plate. The black line represents the reference solution, whereas the red dots are the stress values estimated through the global/local approach in an EW manner. It is important to note that the shear stress value decreases to zero for a ratio x/h equal to 1, revealing that the free-edge effects are confined in a very small region, with dimensions comparable to the plate thickness. For this reason, the EW approach is sufficient for accurately predicting the σ_{yz} at the free-edge and its evolution along the x-direction.

Nevertheless, the free-edge singularities can affect transverse stress values along a larger span length. In this situation, the importance of using a PW approach arises. The composite beam investigated in [45] is considered as a further case. Geometry and loading conditions of
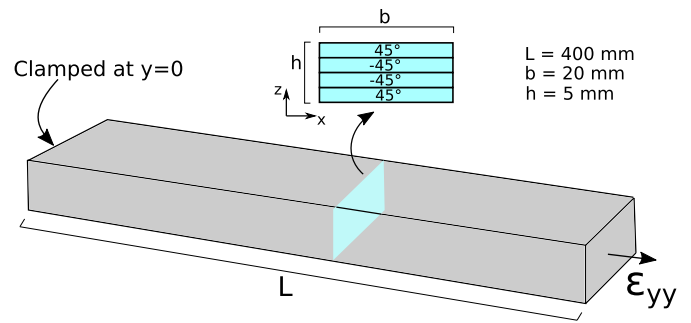

Fig. 23. Geometry and loading conditions of the laminated beam.
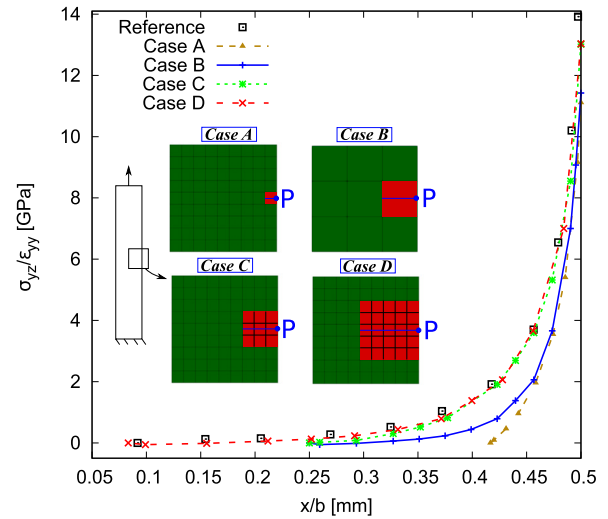

Fig. 24. Transverse shear stress along x at $z = h/4$ and $y = b/2$ for four different models, with the x-axis starting from point P at free-edge and moving towards the center of the plate (blue line). Cases A and B uses EW formulation, whereas cases C and D adopt a PW formulation, with a 3×3 and 5×5 patch, respectively. Reference solution is taken from [46].
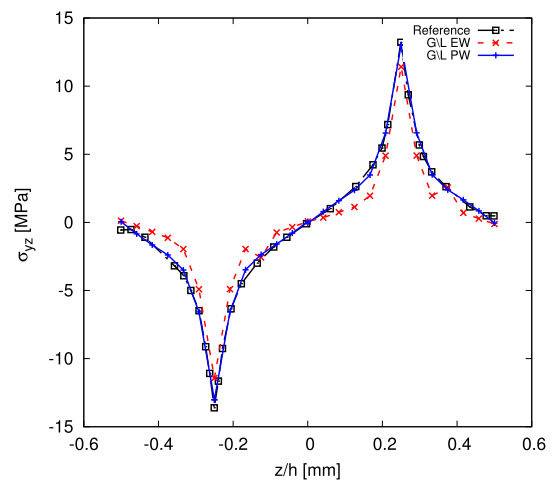
Fig. 25. Transverse shear stresses along z at $y = L/2$ and $x = b$. Reference solution [47] is obtained through a refined LW theory.

the beam are shown in Fig. 23. The laminate has a stacking sequence $[45, -45]_s$, with each layer of equal thickness. A longitudinal strain $\varepsilon_{yy} = 0.01$ is applied to the structure.

Fig. 24 shows the transverse shear stress at $y = l/2$ and at $z = h/4$, from the free-edge ($x/b = 0.5$) towards the center of the plate, along the blue line. Solutions from four different test cases are compared with the

Fig. 26. Transverse shear stresses along z (a) at free-edge, $y = L/2$ and $x/b = 0.5$ and (b) and far from the border, $y = L/2$ and $x/b = 0.45$, using different thickness expansion functions.

approximated elasticity solutions of Pipes and Pagano [46]. Cases A and B use EW approaches with a fine and coarse global mesh. For models C and D, a PW formulation with a 3×3 and a 5×5 patch is adopted in combination with the mo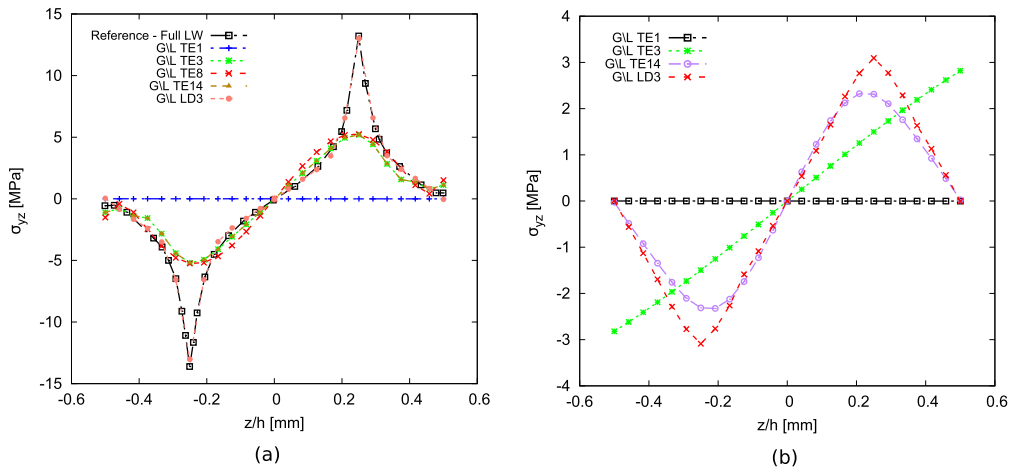st refined global mesh. For all four cases, a 5×5 Q16 mesh is employed for the in-plane discretization of the local model, whereas 8 LD3 are adopted for the through-the-thickness mesh, two for each layer.

For the sake of completeness, the transverse shear stress evolution through the thickness of the plate is displayed in Fig. 25. The results obtained with the present global/local approach, with both EW and PW formulations, are compared with a reference solution [47], where a refined LW theory of structure based on Legendre polynomials is adopted.

Furthermore, Fig. 26 illustrates the effect of theory order adopted through the thickness of the plate on the stress evaluation (a) in the free-edge and (b) in a point far from the border.

The results suggest the following considerations:

- A PW formulation is needed to accurately describe the stress value at the free-edge and the evolution along the span length. In fact, EW models (cases A and B) show some discrepancies in reproducing the reference value for the transverse shear stress, which are correctly replicated when PW models are employed (cases C and D).
- In this particular case, the free-edge phenomenon affects the transverse stress in a relatively vast region, thus making the EW approach not suitable. In fact, model A can calculate σ_{yz} up to $x/b = 0.41$, where a value of zero stress is retrieved. A possible solution could include a coarser global mesh discretization, as in case B. However, a discrepancy with the reference solution is still evident even if the stress can be evaluated until $x/b = 0.25$. Consequently, using a PW model helps in both accuracy and solution field interval. Note that the local region dimensions for cases B and C are the same, with a clear gain in accuracy provided by adopting a 3×3 patch.
- Fig. 26 demonstrates that a layer-wise discretization is needed to describe complex 3D phenomena, such as the free-edge effects occurring in composite laminates. In fact, Fig. 26 (a) shows the transverse shear stress σ_{yz} through the thickness at free edge by using different expansion function in the thickness direction for the local model. It is evident that the use of Taylor expansion, resulting in Equivalent Single Layer (ESL) shear deformation theories, is not sufficient for accurate description of free-edge stresses. On the other hand, Fig. 26 depicts the transverse shear stress at $x/b = 0.45$. In this case, by increasing the order of the Taylor polynomial used for thickness expansion, one is able to retrieve with good accuracy the results provided by the model with layerwise discretization.
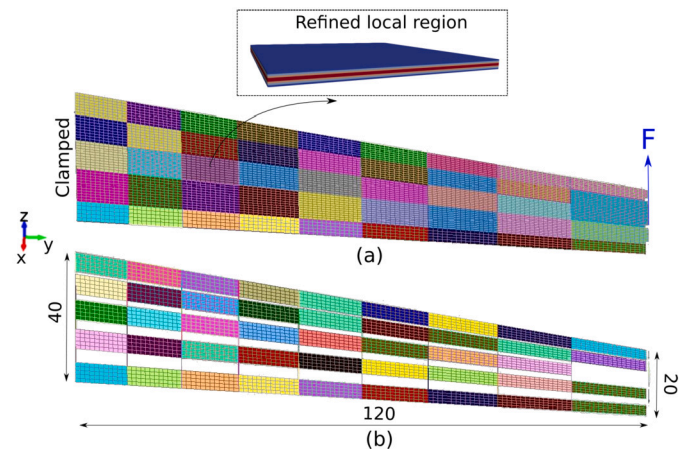

Fig. 27. Geometry and dimensions (in inches) of the wing. The panel chosen as local region is indicated and its 3D representation is also shown.

Table 4
Material properties in Msi.

E_{11}	E_{22}	E_{33}	v_{12}	v_{13}	v_{23}	G_{12}	G_{13}	G_{23}
21.5	1.23	1.23	0.329	0.329	0.329	0.571	0.571	0.571

3.4. Aeronautical wing under bending load

The last numerical example highlights the capability of the proposed approach to deal with complex structures. An aeronautical wing is considered. A graphical representation is shown in Fig. 27. Fig. 27(a) depicts the wing and its upper skin, whereas Fig. 27(b) shows the inner core of the wing, more specifically spars and ribs. The wing has a sweep angle $\Lambda = 16.2°$ and a negative dihedral angle $\Gamma = 1.2°$. It should be noticed that each color could represent a region with different properties, such as thickness and stacking sequence. However, in this example both lower and upper skin structures are made of the same orthotropic material, whose properties are provided in Table 4. The internal reinforcements in both longitudinal and transversal directions are made of aluminum, with $E = 10$ Msi and $v = 0.3$. The total thickness of these reinforcements is equal to 0.1 in. The wing is clamped at one edge, whereas a vertical force of magnitude 15 lbf is applied at the opposite edge.

The global Nastran model is made of 14935 CQUAD4 elements. The selected region for the local analysis is illustrated in Fig. 27, and refers
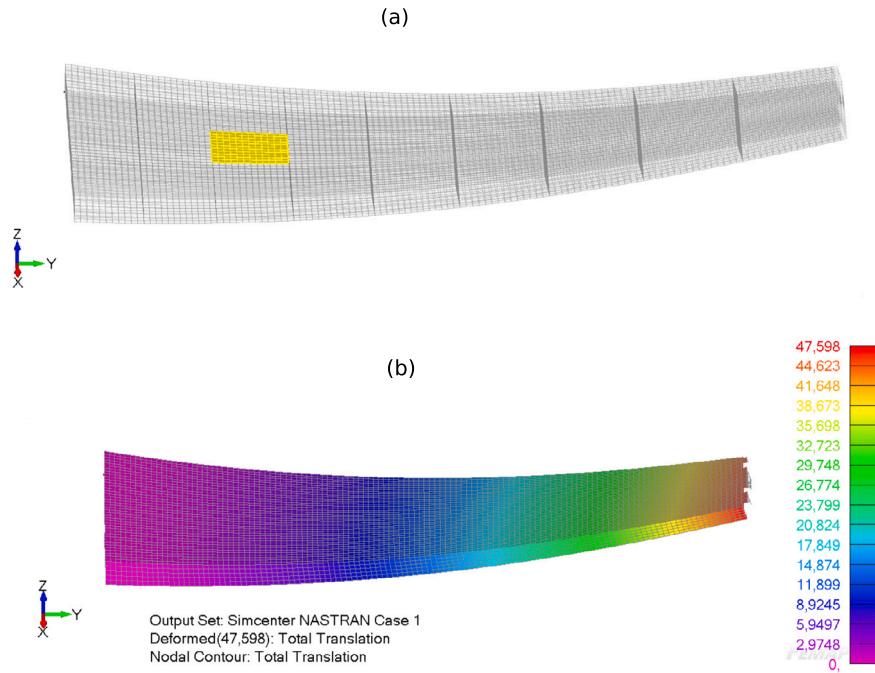
(a)

(b)

| 47,598 |
| 44,623 |
| 41,648 |
| 38,673 |
| 35,698 |
| 32,723 |
| 29,748 |
| 26,774 |
| 23,799 |
| 20,824 |
| 17,849 |
| 14,874 |
| 11,899 |
| 8,9245 |
| 5,9497 |
| 2,9748 |
| 0, |

Output Set: Simcenter NASTRAN Case 1
Deformed(47,598): Total Translation
Nodal Contour: Total Translation

Fig. 28. The chosen patch to be locally refined is highlighted (a), whereas in (b) the deformed configuration of the wing under bending load is shown.
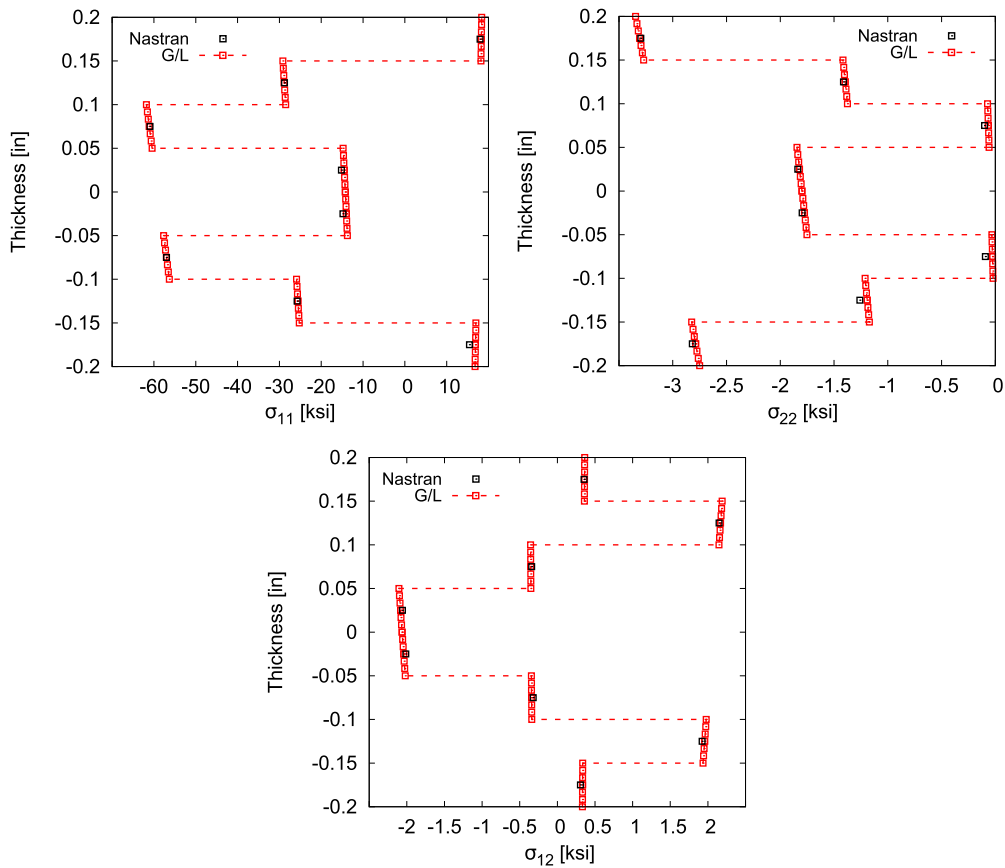

Fig. 29. Comparison of in-plane stresses distribution through the thickness of the wing panel between Nastran simulation and the global/local approach. The stresses are considered in the material reference system.

to a panel in the upper skin. A total of 121 global elements are then considered as local region. The stacking sequence is $[90/45/0/-45]_s$ with respect to the leading edge. Finally, each ply has a thickness of 0.05 in. The refined region is discretized with a 5×5 grid of cubic Q16

elements, whereas a total of 16 LD3 element are adopted through the thickness, two for each layer.

Fig. 28 illustrates the chosen patch for the local analysis on the global model and the behavior of the wing under bending load.
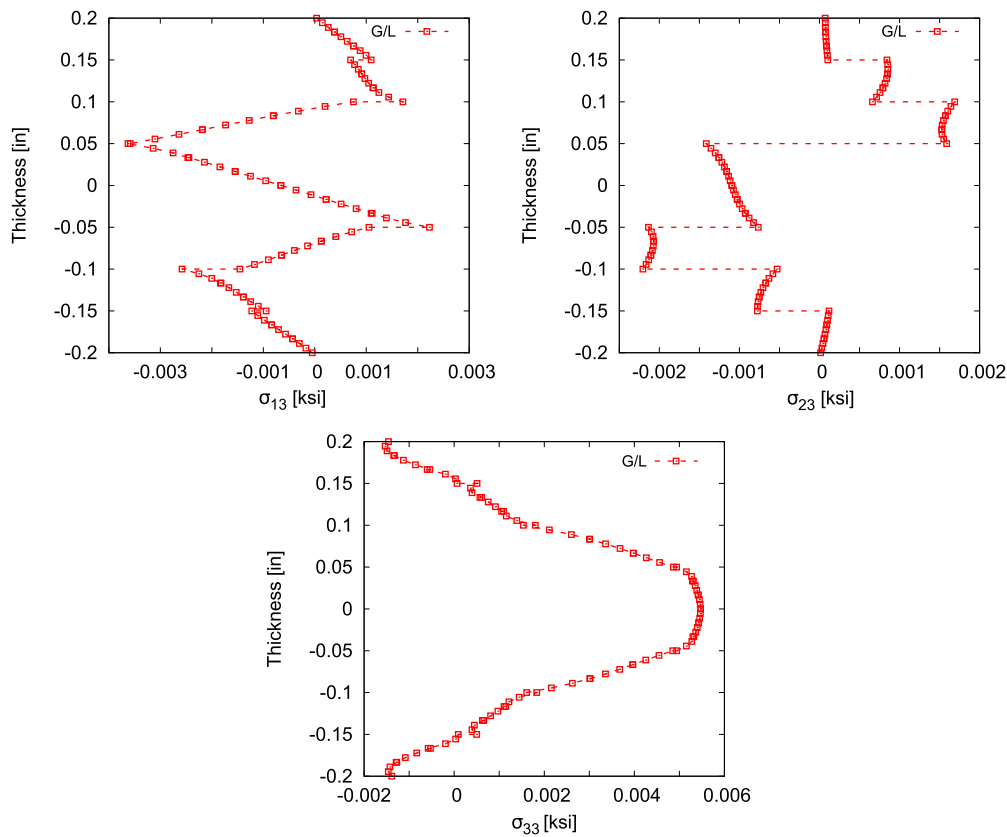
Fig. 30. Transverse stresses distribution through the thickness of the wing panel evaluated with the global/local approach. The stresses are considered in the material reference system.

Table 5
Material allowables in ksi.

X_T	X_C	Y_T	Y_C	XY	XZ	YZ
477.0	216.1	11.0	40.3	20.0	19.1	20.0

The solution from the global/local analysis is compared with the results coming from the stress computation in Nastran at global scale. The evaluation is made in the central point of the investigated panel. Fig. 29 shows the in-plane stresses distribution through the thickness of the wing panel, demonstrating an accurate match with the solution retrieved from the global analysis. For the sake of completeness, Fig. 30 illustrates the transverse stresses obtained with the global/local approach, expressed with respect to the global reference system.

Furthermore, a failure index evaluation is performed on the investigated panel. As previously done in Section 3.1, an Hashin-based criterion is adopted. The material allowables are presented in Table 5. The Hashin criterion is able to distinguish between four failure modes. Their distributions through the thickness of the panel in its central point are depicted in Fig. 31. The outcome shows that the maximum value of failure index is found for the fiber compression mode in the layers with fiber oriented in the same direction as the leading edge, thus respecting the physics of the problem.

4. Conclusions

This work establishes a one-way coupling global/local approach for accurately analyzing 3D stress states in a composite laminate. The global analysis is performed through finite element models using classical plate elements in Nastran, whereas the local model is built by means of the Carrera Unified Formulation (CUF). This technique allows the development of higher-order plate models to describe selected do-
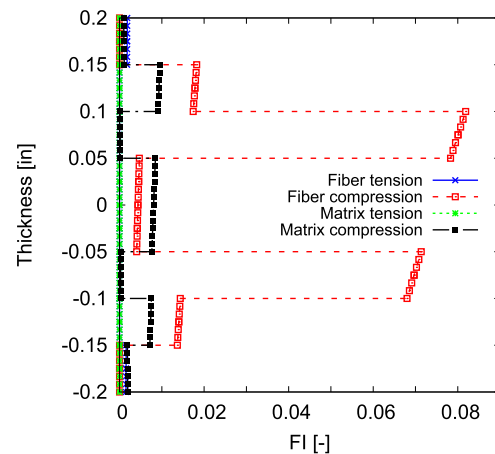

Fig. 31. Hashin-based failure indices in the investigated wing panel.

mains of the global structure. The main novelty of the present work is the extension from an element-wise (EW) to a patch-wise (PW) formulation. According to the EW formulation, only one 2D element from the global structure is chosen to be locally analyzed. The extension to the PW formulation opens the possibility of selecting a set of elements and, consequently, a larger domain. EW and PW approaches are compared with stress states obtained through a full layer-wise (LW) model. Results show that the EW formulation is insufficient for the correct recovery of the 3D stress state through the thickness of the laminate, especially when transverse shear stresses are considered. A complete convergence study on mesh refinement for both global and local models is conducted. Moreover, this study highlights the necessity of the PW formulation to correctly evaluate the free-edge effects,

which is a common phenomenon in composite laminates. Finally, a wing structure is considered as last numerical example to demonstrate the capability of the present approach to deal with complex structure. The extension to the PW formulation will enable the possibility of embedding this global/local technique in more complex procedures, such as least-weight design of large heterogeneous complex assemblies, stiffness optimization or localized progressive failure analysis in structures of relevant interest.

CRediT authorship contribution statement

M. Enea: Formal analysis, Investigation, Software, Visualization, Writing – original draft. **R. Augello:** Methodology, Software, Validation, Writing – review & editing. **A. Pagani:** Funding acquisition, Methodology, Resources, Supervision, Writing – review & editing. **E. Carrera:** Funding acquisition, Methodology, Supervision, Writing – review & editing.

Declaration of competing interest

The authors declare that they have no known competing financial interests or personal relationships that could have appeared to influence the work reported in this paper.

Data availability

Data will be made available on request.

Acknowledgements

References

[1] De Miguel A, Kaleel I, Nagaraj M, Pagani A, Petrolo M, Carrera E. Accurate evaluation of failure indices of composite layered structures via various FE models. Compos Sci Technol 2018;167:174–89.

[2] Hirai I, Wang B, Pilkey W. An efficient zooming method for finite element analysis. Int J Numer Methods Eng 1984;20:1671–83.

[3] Ransom JB, Knight Jr NF. Global/local stress analysis of composite panels. Comput Struct 1990;37(4):375–95.

[4] Mao KM, Sun CT. A refined global-local finite element analysis method. Int J Numer Methods Eng 1991;32(1):29–43.

[5] Whitcomb JD. Iterative global/local finite element analysis. Comput Struct 1991;40(4):1027–31.

[6] Noor AK. Global-local methodologies and their application to nonlinear analysis. Finite Elem Anal Des 1986;2(4):333–46.

[7] Whitcomb J, Woo K. Global/local finite element analysis of geometrically nonlinear structures. In: 33rd structures, structural dynamics and materials conference; 1992. p. 2236.

[8] Babuška I, Chandra J, Flaherty J. Adaptive computational methods for partial differential equations, vol. 16. SIAM; 1983.

[9] Babuska I, Szabo BA, Katz N. The p-version of the finite element method. SIAM J Numer Anal 1981;18(3):515–45.

[10] Babuška I, Dorr M. Error estimates for the combined h and p versions of the finite element method. Numer Math 1981;37(2):257–77.

[11] Hühne S, Reinoso J, Jansen E, Rolfes R. A two-way loose coupling procedure for investigating the buckling and damage behaviour of stiffened composite panels. Compos Struct 2016;136:513–25.

[12] Akterskaia M, Jansen E, Hühne S, Rolfes R. Efficient progressive failure analysis of multi-stringer stiffened composite panels through a two-way loose coupling global-local approach. Compos Struct 2018;183:137–45.

[13] Akterskaia M, Jansen E, Hallett S, Weaver P, Rolfes R. Analysis of skin-stringer debonding in composite panels through a two-way global-local method. Compos Struct 2018;202:1280–94.

[14] Krueger R, O'Brien K. A shell/3D modeling technique for the analysis of delaminated composite laminates. Composites, Part A, Appl Sci Manuf 2001;32(1):25–44.

[15] Krueger R, Minguet P. Analysis of composite skin–stiffener debond specimens using a shell/3D modeling technique. Compos Struct 2007;81(1):41–59.

[16] Sun X, Hallett S. Barely visible impact damage in scaled composite laminates: experiments and numerical simulations. Int J Impact Eng 2017;109:178–95.

[17] Riccio A, De Luca A, Di Felice G, Caputo F. Modelling the simulation of impact induced damage onset and evolution in composites. Composites, Part B, Eng 2014;66:340–7.

[18] Fish J, Pan L, Belsky V, Gomaa S. Unstructured multigrid method for shells. Int J Numer Methods Eng 1996;39(7):1181–97.

[19] Dhia HB. Multiscale mechanical problems: the arlequin method. C R Acad. Sci, Sér 2B, Méc Phys Astron 1998;12(326):899–904.

[20] Labeas G, Belesis S, Diamantakos I, Tserpes K. Adaptative progressive damage modeling for large-scale composite structures. Int J Damage Mech 2012;21(3):441–62.

[21] Gendre L, Allix O, Gosselet P, Comte F. Non-intrusive and exact global/local techniques for structural problems with local plasticity. Comput Mech 2009;44(2):233–45.

[22] Vescovini R, Davila C, Bisagni C. Failure analysis of composite multi-stringer panels using simplified models. Composites, Part B, Eng 2013;45(1):939–51.

[23] Orifici A, Thomson R, Herszberg I, Weller T, Degenhardt R, Bayandor J. An analysis methodology for failure in postbuckling skin–stiffener interfaces. Compos Struct 2008;86(1–3):186–93.

[24] Reddy JN. Mechanics of laminated composite plates and shells: theory and analysis. CRC Press; 2003.

[25] Silva G, Do Prado A, Cabral P, De Breuker R, Dillinger J. Tailoring of a composite regional jet wing using the slice and swap method. J Aircr 2019;56(3):990–1004.

[26] Carrera E, Cinefra M, Petrolo M, Zappino E. Finite element analysis of structures through unified formulation. John Wiley & Sons. ISBN 978-1-119-94121-7, 2014.

[27] Sánchez-Majano AR, Azzara R, Pagani A, Carrera E. Accurate stress analysis of variable angle tow shells by high-order equivalent-single-layer and layer-wise finite element models. Materials 2021;14(21):6486.

[28] De Miguel A, Pagani A, Carrera E. Free-edge stress fields in generic laminated composites via higher-order kinematics. Composites, Part B, Eng 2019;168:375–86.

[29] Carrera E, de Miguel A, Filippi M, Kaleel I, Pagani A, Petrolo M, et al. Global-local plug-in for high-fidelity composite stress analysis in femap/NX nastran. Mech Adv Mat Struct 2021;28(11):1121–7.

[30] Carrera E, De Miguel AG, Filippi M, Kaleel I, Pagani A, Petrolo M, et al. Global-local plug-in for high-fidelity composite stress analysis in ABAQUS. Mech Adv Mat Struct 2021;28(14):1445–50.

[31] Vijayachandran AA, Waas AM. Minimizing stress concentrations using steered fiber-paths and incorporating realistic manufacturing signatures. Int J Non-Linear Mech 2022;146:104160.

[32] Pagani A, Carrera E. Coupling 3D peridynamics and high order 1D finite elements based on local elasticity for the linear static analysis of solid beams and thin-walled reinforced structures. Int J Numer Methods Eng 2020;121.

[33] Scabbia F, Enea M. An improved coupling of 3D state-based peridynamics with high-order 1d finite elements to reduce spurious effects at interfaces. Int J Numer Methods Eng 2023.

[34] Pagani A, Enea M, Carrera E. Quasi-static fracture analysis by coupled three-dimensional peridynamics and high order one-dimensional finite elements based on local elasticity. Int J Numer Methods Eng 2022;123(4):1098–113.

[35] MacNeal RH. The NASTRAN theoretical manual, vol. 221. Scientific and Technical Information Office, National Aeronautics and Space; 1970.

[36] Reissner E, Stavsky Y. Bending and stretching of certain types of heterogeneous aeolotropic elastic plates. J Appl Mech 1961;28:402–8.

[37] Augello R, Pagani A, Carrera E, Iannotta A. Stress and failure onset analysis of thin composite deployables by global/local approach. AIAA J 2022:1–13.

[38] Oñate E. Structural analysis with the finite element method: linear statics, vol. 1. Springer; 2009.

[39] Reissner E. The effect of transverse shear deformation on the bending of elastic plates. J Appl Mech 1945;12(2):A69–77.

[40] Mindlin R. Influence of rotatory inertia and shear on flexural motions of isotropic, elastic plates. Trans ASME Appl Mech 1951;18:31–8.

[41] Wright K. Chebyshev collocation methods for ordinary differential equations. Comput J 1964;6(4):358–65.

[42] Carrera E. Historical review of zig-zag theories for multilayered plates and shells. Appl Mech Rev 2003;56(3):287–308.

[43] Hashin Z. Failure criteria for unidirectional fiber composites. J Appl Mech 1980;47(2):329–34.

[44] Lorriot TH, Marion G, Harry R, Wargnier H. Onset of free-edge delamination in composite laminates under tensile loading. Composites, Part B, Eng 2003;34(5):459–71.

[45] Pipes RB, Pagano NJ. Interlaminar stresses in composite laminates under uniform axial extension. J Compos Mater 1970;4(4):538–48.

[46] Pipes RB, Pagano NJ. Interlaminar stresses in composite laminates—an approximate elasticity solution. J Appl Mech 1974;41(3):668–72.

[47] de Miguel AG, Carrera E, Pagani A, Zappino E. Accurate evaluation of interlaminar stresses in composite laminates via mixed one-dimensional formulation. AIAA J 2018;56:1–13.